Atmos. Chem. Phys. Discuss., 12, 6593–6622, 2012
www.atmos-chem-phys-discuss.net/12/6593/2012/
doi:10.5194/acpd-12-6593-2012

Atmospheric Chemistry and Physics Discussions

Aerosol radiative forcing during African desert dust events (2005–2010) over South-Eastern Spain

A. Valenzuela[1,2], **F. J. Olmo**[1,2], **H. Lyamani**[1,2], **M. Antón**[1,2], **A. Quirantes**[1], and **L. Alados-Arboledas**[1,2]

[1]Departamento de Física Aplicada, Universidad de Granada, Granada, Spain
[2]Centro Andaluz de Medio Ambiente (CEAMA), Granada, Spain

Received: 23 January 2012 – Accepted: 22 February 2012 – Published: 2 March 2012

Correspondence to: A. Valenzuela (avalenzuela@ugr.es)

Published by Copernicus Publications on behalf of the European Geosciences Union.

Abstract

The instantaneous values of the aerosol radiative forcing (ARF) at the surface and the top of the atmosphere (TOA) were calculated during desert dust events occurred at Granada (Southeastern Spain) from 2005 to 2010. For that, the SBDART radiative transfer model was utilized to simulate the global irradiance values (0.3–2.8 µm) at the surface and TOA using as input the aerosol properties derived from a CIMEL sun-photometer measurements and an inversion methodology that uses the sky radiance measurements in principal plane configuration and non-spherical particle shapes approximation. The SBDART modeled global irradiances at surface have been successfully validated against experimental measurements obtained by CM-11 pyranometer, indicating the reliability of the radiative transfer model used in this work for the ARF calculations.

The monthly ARF values at surface ranged from $-32\,W\,m^{-2}$ to $-46\,W\,m^{-2}$, being larger in April and July than in the rest of months. The seasonal ARF evolution was inconsistent with seasonal aerosol optical depth (AOD) variation due to the effects induced by other aerosol parameter such as the single scattering albedo. The ARF at TOA changed from $-9\,W\,m^{-2}$ to $-29\,W\,m^{-2}$. Thus, the atmospheric ARF values (ARF at TOA minus ARF at surface) ranged from +15 to $+35\,W\,m^{-2}$. These results suggest that the African dust caused local atmospheric heating over the study location.

The instantaneous aerosol radiative forcing efficiency (ARFE), aerosol radiative forcing per unit of AOD (440 nm), at surface and TOA during African desert dust events was evaluated according to the desert dust source origins. The ARFE values at surface were relatively high (in absolute term) and were -157 ± 20 (Sector A), -154 ± 23 (Sector B), and -147 ± 23 (Sector C) $W\,m^{-2}$. These values were larger than many of the values found in literature which could be due to the presence of more absorbing atmospheric particles during African desert dust intrusions over our study area. Finally, our ARF computations showed good agreement with the corresponding ARF calculated by AERONET network.

ACPD

12, 6593–6622, 2012

1 Introduction

Mineral dust particles are one of the main constituents of the atmospheric aerosol determining the radiation budget of the atmosphere. The evaluation of the dust-radiation interaction is essential for climate forcing assessment at both local and regional scales. However, large uncertainties still remain in assessing the dust climate impacts (Foster et al., 2007). To understand the radiative effects of dust it is crucial to characterize its optical properties. One of the major sources of the large uncertainties in dust radiative forcing is associated with dust optical and physical properties due to the complexity in dust size distribution, morphology, and mineral composition (Sokolik and Toon, 1999).

The Sahara desert is the most important source of mineral dust in the Northern Hemisphere (e.g., Prospero et al., 2002). North African dust is injected into the atmosphere through resuspension processes at the source areas, being transported at different altitudes (up to 7 km) to different areas in the world (e.g., Tesche et al., 2009). Papayannis et al. (2008) performed more than 130 observation days of the horizontal and vertical extent of Saharan dust intrusions over Europe by means of a coordinated lidar network in the frame of the European Aerosol Research Lidar Network (EARLINET). They found that Saharan dust source regions play a key role in the dust transport to Europe in the height region between 3 and 5 km.

The Iberian Peninsula is frequently affected by African dust intrusions with large aerosol load that modulate the aerosol climatology in different areas of this region, especially in the South of Spain (Toledano et al., 2007; Cachorro et al., 2008) and Portugal (Wagner et al., 2009). The sign and magnitude of the ARF associated with these intrusions depends on the dust particles scattering and absorbing properties which are controlled by a number of parameters such as dust size distribution, chemical composition, particles mixing state as well as particle shapes (Otto et al., 2009). Close to the source region mostly pure dust is found, but after a long range transport the aging of the dust and mixing with other aerosol types modify the optical properties of the desert dust (Bauer et al., 2011). Several works have shown that mineral dust in

ACPD
12, 6593–6622, 2012

the atmosphere is often mixed with anthropogenic aerosol (e.g., Kandler et al., 2007; Gangoiti et al., 2006). Recently, Rodríguez et al. (2011) showed that anthropogenic emissions from crude oil refineries and power plants, located in North African urban areas contribute to desert dust mixing with particulate pollutants. Hence, the contribution of anthropogenic particles emitted in urban areas located in North Africa can be relevant during African dust events over Mediterranean sites which is supported by the relatively high Angstrom exponent (α) values measured during these events in comparison to those obtained in areas close to the dust sources and by the results obtained from the analysis of the chemical composition of ground collected particles (Bellantone et al., 2008; Carofalo et al., 2008). Thus, several authors have pointed out the importance of taking into account the influence of the anthropogenic particles on the direct radiative forcing associated with African desert dust intrusions over the Mediterranean basin and continental Europe (e.g., Gerasopoulos et al., 2003; Perrone and Bergamo, 2011).

In a recent paper, Valenzuela et al. (2012a) have analyzed the columnar aerosol radiative properties during African dust intrusions over Granada, reporting values of the single scattering albedo, $\omega_o(\lambda)$, smaller than those found in other locations which were explained by the mixing of desert dust with absorbing particles from anthropogenic origin. Knowledge of the absorption variability of these aerosol mixtures is particularly important for assessing the direct radiative forcing of these aerosol types (Garcia et al., 2011).

The shapes of dust particles are exclusively irregular (Koren et al., 2001; Muñoz et al., 2001), and the theoretical studies of dust optical properties based on a spheroid polydispersion model have shown that dust properties can be substantially different to those obtained with Lorenz-Mie theory adopting spherical model (Mishchenko et al., 1997). These last authors found that the spherical particle approximation is probably among the major sources of error in quantifying the radiative forcing effect of mineral particles. Otto et al. (2009) stated that certain spheroidal shape parameterizations can substantially diminish the differences between the experimental and modeled values

ACPD
12, 6593–6622, 2012

of the atmospheric aerosol radiative forcing. Yang et al. (2007) estimated the influence of prolate spheroidal model particles on the radiation field and stated that the non-sphericity of particles affects the short-wave radiation significantly, but has no impact on the long-wave radiation. Pilinis and Li (1998) estimated the radiative forcing of prolate spheroidal model particles and found that this assumption can result in a radiative forcing which is different by a factor of 3 compared to spherical particles shape assumption. Also, they found that the consideration of particle shape is important for the upwelling scattered radiation, especially for small solar zenith angles and super-micron-sized particles, and that the upward scattered radiation is underestimated when adopting spherical particles assumption. For this reason, for calculating the aerosol radiative forcing during desert dust intrusions analyzed in this study we used the aerosol optical properties retrieved by an inversion method that take into account the non-sphericity of dust particles (Olmo et al., 2008).

During the last years different authors have proposed codes for the retrieval of the aerosol microphysical properties using sun and sky radiance measurements in the almucantar and/or principal plane configurations (e.g., Nakajima et al., 1996; Vermeulen et al., 2000; Dubovik and King, 2000; Dubovik et al., 2002a, 2006; Olmo et al., 2006, 2008). Using these tools many authors have presented results of columnar aerosol optical and microphysical properties retrieved using sky radiance sun-photometric measurements in the almucantar configuration (e.g., Dubovik et al., 2002b; Kubilay et al., 2003; Lyamani et al., 2006b; Tafuro et al., 2006; Olmo et al., 2006; Cachorro et al., 2008; Pinker et al., 2010; Eck et al., 2010; Garcia et al., 2011). However, only a few authors have presented results of aerosol optical properties retrieved using sky radiance measurements in the principal plane configuration (e.g., Li et al., 2004; Dubovik et al., 2006; Olmo et al., 2008; Valenzuela et al., 2012a,b). Sky radiance measurements in the solar principal plane have received less attention than almucantar sky radiance measurements, likely due to the fact that while almucantar retrievals are routinely computed and distributed by AERONET the principal plane retrievals are not publicly available. The sky radiance measurements in principal plane configuration

ACPD
12, 6593–6622, 2012

allows us to obtain columnar optical and microphysical aerosol properties along the day, not just for large solar zenith angles as when we use sky radiance measurements in the almucantar configuration. In this study, for calculating the aerosol radiative forcing during desert dust intrusions over Granada, we used the aerosol optical properties retrieved by the principal plane inversion method of Olmo et al. (2008). This inversion method spheroid models to account for aerosol particle nonsphericity.

The main objective of this work is to evaluate the instantaneous aerosol radiative forcing at surface and TOA during African desert dust intrusions occurred at Granada (South-Eastern Spain) from 2005 to 2010. In addition, the aerosol radiative forcing per unit of aerosol optical depth (aerosol radiative forcing efficiency) during these intrusions is also analyzed according to the desert dust source origins.

This paper is structured as follows: Sect. 2 present the experimental site and the instrumentation used. Section 3 describes briefly the methodology used. Section 4 discusses the results and the validation of the modeled irradiances. Section 5 summarizes the main conclusions.

2 Experimental site and instrumentation

The instruments used in this study are installed in the Andalusian Center for Environmental Studies (CEAMA) in the urban area of Granada (37.16° N, 3.61° W and 680 m a.s.l.). Granada, located in South-Eastern Spain, is a non-industrialized, medium-sized city with a population of 300 000. The city is situated in a natural basin surrounded by mountains with altitudes over 1000 m. The near-continental conditions prevailing at this site are responsible for large seasonal temperature differences, providing cool winters and hot summers. The study area also experiences periods of low humidity regime especially at summer time. The study area is about 200 km away from the African continent, and approximately 50 km away from the Western Mediterranean Basin. Due to its proximity to the African continent our study area is usually affected by African dust intrusions (e.g., Lyamani et al., 2005, 2006a; Olmo et al., 2006, 2008).

ACPD
12, 6593–6622, 2012

Column-integrated characterization of the atmospheric aerosol has been performed by means of a sun-photometer CIMEL CE-318-4 included in the AERONET network (Holben et al., 1998). This sun-photometer makes direct sun measurements with a 1.2° full field of view at 340, 380, 440, 670, 500, 870, 940 and 1020 nm. The full-width at half-maximum of the interference filters are 2 nm at 340 nm, 4 nm at 380 nm and 10 nm at all other wavelengths. In addition, the CIMEL instrument performs sky radiances, both in almucantar and principal plane configurations, at 440, 670, 870 and 1020 nm. Calibration of this instrument was performed by AERONET-RIMA network. More details about this instrument are given by Holben et al. (1998).

The ground-based station is equipped with a CM-11 pyranometer manufactured by Kipp & Zonen (Delft, The Netherlands) measuring the SW solar irradiance data (310–3200 nm). The CM-11 pyranometer complies with the specifications for the first-class WMO classification of this instrument (resolution better than $\pm 5\,\mathrm{W\,m^{-2}}$), and the calibration factor stability has been periodically checked against a reference CM-11 pyranometer.

3 Methodology and data

3.1 Aerosol optical properties data

In this study, aerosol optical and microphysical properties (spectral aerosol optical depth (AOD(λ)), spectral single scattering albedo ($\omega_{0A}(\lambda)$) and spectral asymmetry parameter $g(\lambda)$) obtained by sun photometer CIMEL during Saharan desert dust intrusions over Granada area are used. These data were presented and analyzed in more detail by Valenzuela et al. (2012a,b). In addition, these authors have classified these aerosol properties according to desert dust origin in three sectors; sector A (North Morocco, Northwest Algeria), sector B (Western Sahara, Northwest Mauritania and Southwest Algeria) and sector C (Eastern Algeria, Tunisia).

ACPD
12, 6593–6622, 2012

The aerosol optical depths, at the selected spectral channels, have been computed using the sun-photometer solar extinction measurements and the calibration constants provided by AERONET following the method described in the works of (Alados-Arboledas et al., 2003, 2008). The spectral single scattering albedo and asymmetry parameter were retrieved using solar extinction measurements in combination with principal plane sky radiance measurements by the inversion method of Olmo et al. (2008). This method has been previously described (Olmo et al., 2008) and successfully used in different studies (e.g., Valenzuela et al., 2012a,b). This inversion method is an improvement of the original method of Nakajima et al. (1996). The most important improvement in this method is the substitution of spherical model used in the original algorithm by spheroid model to account for aerosol particle nonsphericity in remote sensing of desert dust (Olmo et al., 2008). This inversion procedure uses as input parameters the spectral AOD and the normalized spectral sky radiances. Sensitivity tests of the inversion code and comparison with the AERONET results in different atmospheric conditions showed agreements and that the errors do not significantly affect the derivation of the main features of the aerosol properties. More detail about this inversion method is given by Olmo et al. (2008).

3.2 Aerosol radiative forcing determination

Aerosol radiative forcing (ARF) at surface (at TOA) is defined as the instantaneous increase or decrease of the net radiation flux at the surface (at TOA) that is due to an instantaneous change of aerosol atmospheric content. The atmospheric ARF is defined as the radiative forcing at TOA minus the radiative forcing at the surface.

In this study, we have chosen the atmosphere free of aerosols as the reference case. Thus, the instantaneous values of ARF can be derived from the following expression (Meloni et al., 2005):

$$\mathrm{ARF} = \left(F^{\downarrow} - F^{\uparrow}\right) - \left(F_0^{\downarrow} - F_0^{\uparrow}\right) \quad (1)$$

ACPD
12, 6593–6622, 2012

where F and F_0 denote the global irradiances with aerosol and without aerosol, respectively. The arrows indicate the direction of the global irradiances, ↓ indicating downward irradiance and ↑ indicating upward irradiance.

To carry out the instantaneous global solar irradiances computations we have used the radiative transfer computer code SBDART (Ricchiazzi et al., 1998), which is a discrete ordinates radiative transfer model (Stamnes et al., 1988). This algorithm includes multiple scattering in a vertically inhomogeneous non-isothermal plane-parallel media, and it has been shown to be computationally efficient and to reliably resolve the radiative transfer equation. This radiative transfer computer code characterizes the atmospheric aerosol radiative effects using as input the solar zenith angle, the spectral aerosol optical depth, the spectral single scattering albedo, and the spectral asymmetry parameter. In this study, we used the spectral aerosol optical depth, the spectral single scattering albedo, and the spectral asymmetry parameter obtained by the CIMEL sun- photometer which were presented and analyzed in more detail by Valenzuela et al. (2012a,b). Other parameters used by the code are the spectral solar radiation, surface height, total ozone columnar concentration taken from TOMS satellite (http://ozoneaq.gsfc.nasa.gov/), surface albedo fixed to 0.15 in study area, the model atmosphere (in our case midlatitude with seasonal dependence), and stratospheric aerosol (not assumed in our case). The output parameters of the code are the downward and the upward global irradiance at surface and at TOA. Calculations were performed and integrated over the 0.31–2.8 µm solar spectral range for solar zenith angles varying from 20° to 80°.

In order to analyze the relative differences between the experimental and modeled values, the statistical relative parameters MBE (mean bias error) and MABE (mean absolute bias error) were calculated as follows:

$$\mathrm{MBE}(\%) = \frac{100}{N} \sum_{i=1}^{N} \frac{F_i^{\mathrm{mod}} - F_i^{\mathrm{exp}}}{F_i^{\mathrm{exp}}} \quad (2)$$

ACPD
12, 6593–6622, 2012

$$\mathrm{MABE}(\%) = \frac{100}{N}\sum_{i=1}^{N}\frac{\left|F_i^{\mathrm{mod}} - F_i^{\mathrm{exp}}\right|}{F_i^{\mathrm{exp}}} \quad (3)$$

where F_i^{mod} and F_i^{exp} are the modeled and experimental global irradiances and N is the total number of data. While the MBE parameter shows the degree of underestimation or overestimation of the SBDART simulations with respect to the experimental measurements, the MABE parameter reports about the absolute value of the relative differences between modeled and measured data.

4 Results and discussion

The simulated net irradiances at surface and TOA during desert dust intrusions occurred at Granada from 2005 to 2010 have been obtained using as input in the SBDART radiative transfer model the experimental aerosol information (aerosol optical depth, single scattering albedo and asymmetry parameter) derived from the principal plane retrievals. Additionally, the net shortwave irradiances at surface and TOA under a clean atmosphere (cloud-free conditions and no presence of aerosol) have been also derived from the SBDART code. Therefore, a simulated ARF was obtained from equation 1 for the 911 instantaneous measurements obtained during desert dust events occurred at Granada from 2005 to 2010. As we commented before, the spectral aerosol optical properties used as input for SBDART model calculations in this study were analyzed and classified in three groups according to the desert dust origin sources by Valenzuela et al. (2012b).

Firstly, the reliability of the SBDART model was analyzed. For that, we have compared the experimental downward irradiances and the corresponding SBDART simulations for all cases analyzed in this study. Figure 1 shows three plots with the correlation between the measured and simulated values for the three desert dust origin classes; sector A (North Morocco, Northwest Algeria), sector B (Western Sahara, Northwest

ACPD
12, 6593–6622, 2012

Mauritania and Southwest Algeria) and sector C (Eastern Algeria, Tunisia). The solid line represents the zero bias line (slope equal to one) which fits the data well, confirming the high degree of agreement. A linear regression analysis between the measured and the modeled downward irradiances has been performed. The correlation coefficient values were higher than 0.98, indicating that the measured and modeled values were well correlated in the three dust origin classes. The statistical analysis gives slopes very close to unity, supporting the validity of the radiative transfer model computations of ARF presented in this work.

The results indicate that the radiative transfer model slightly overestimates the experimental global irradiance with MBE values of +2.9, +1.7 and +2.4 % for sector A, sector B and sector C, respectively. These small discrepancies could be associated with errors in the model input parameters as well as errors in the experimental measurements of the global irradiance. Additionally, these differences could be partially related to the overestimation of the diffuse component by the SBDART model (Pinker et al., 2010; Won et al., 2004; Kim et al., 2005). The MABE parameter presented values smaller than 4 % for the three sectors, indicating the reliability of the radiative transfer model used in this work for the ARF calculations.

The overall mean ARF at TOA (ARF_{TOA}) during all desert dust events was $(-12 \pm 11)\,W\,m^{-2}$, while the overall mean ARF at surface ($ARF_{Surface}$) was $(-40 \pm 23)\ W\,m^{-2}$, producing an atmospheric mean ARF ($ARF_{Atmosphere}$) value of $(+29 \pm 25)\,W\,m^{-2}$. The negative ARF value at TOA indicates that desert dust aerosol caused an increase of light scattered back to space inducing thus a significant Earth-atmosphere cooling. In addition, the negative value at surface reveals that the desert dust aerosol reduced significantly the solar radiation reaching the ground level producing thus a large surface cooling. This result suggests a relevant absorption of solar radiation in the atmosphere, leading to significant atmospheric warming.

The monthly mean values of ARF at surface and TOA during all desert dust events occurred at Granada from 2005 to 2010 are shown in Fig. 2. Additionally, the atmospheric ARF is also shown in this figure. The ARF values ranged from $-32\,W\,m^{-2}$ to

ACPD
12, 6593–6622, 2012

$-46\,W\,m^{-2}$ at surface, from $-9\,W\,m^{-2}$ to $-29\,W\,m^{-2}$ at TOA and from $+15\,W\,m^{-2}$ to $+35\,W\,m^{-2}$ in the atmosphere. The ARF at surface was slightly larger in April and July than in the rest of months. It is important to note that the monthly ARF at surface did not follow the monthly aerosol optical depth evolution found by Valenzuela et al. (2012a).

In fact, the monthly AOD (440 nm) value was slightly larger in June (0.37) than in July (0.31). However, ARF at surface was larger in July ($-46\,W\,m^{-2}$) than in June ($-39\,W\,m^{-2}$). This inconsistency of ARF with AOD was attributed to the effects induced by other aerosol parameter such as single scattering albedo. In fact, the largest values of ARF at surface in April and July coincided with the lowest monthly values of the single scattering albedo for those months (Valenzuela et al., 2012a). This result is in agreement with the works of Di Biagio et al. (2009) and Antón et al. (2011) that showed that the single scattering albedo has a large influence on the ARF. On the other hand, the ARF at TOA was smaller (in absolute value) for the months between April and August than for the rest of months. The small values of the forcing at TOA during those months and the corresponding high values at the surface mean that less solar energy reached the ground and more energy was absorbed by atmosphere. For this reason, the atmospheric ARF was higher from May to August than the rest of months.

Figure 3 shows ARF at surface and TOA as a function of solar zenith angle (SZA) computed using mean values of the optical properties for each one of the desert dust origin classes. From this figure, the SZA dependence of the ARF at TOA is obvious. Indeed, the ARF increased (in absolute value) as a function of SZA for the three classifications, showing no significant differences each other. Thus, the ARF at TOA changed from $-5\,W\,m^{-2}$ for SZA of 20° to around $-25\,W\,m^{-2}$ for SZA of 70°. As the solar zenith angle increases the ARF tended to increase (absolute value) at TOA up to 70°. As SZA increase a larger portion of the forward hemisphere includes the region of the upwelling scattered irradiance which could explain the increase of ARF as SZA increase. In contrast, the ARF at surface only presented a slight SZA dependence. The ARF increase (absolute value) at surface was due to the increase in photon path length and the associated increase in the attenuation, scattering and absorption, of direct solar

ACPD
12, 6593–6622, 2012

radiation (Meloni et al., 2005). For instance, the ARF ranged from $-40\,W\,m^{-2}$ for SZA of 20° to minimum values of $-50\,W\,m^{-2}$ for SZA of 70°. Additionally, it can be seen that the surface ARF presented larger values (in absolute term) when air masses are transported from sector B. This was consistent with higher value of AOD for this sector showed by Valenzuela et al. (2012b). For SZA greater than 70° the ARF decreased in absolute value with the zenith angle at surface and TOA, being more pronounced at surface. Probably, this could be explained by the long path at high SZA, which includes strong attenuation of direct solar radiation but also more multiple scattering and hence more scattered light. The strong ARF decrease for SZA > 70° at surface could be associated with larger absorption at surface.

Table 1 shows the overall averages (± one standard deviation) of the direct, diffuse and global irradiances at surface simulated by SBDART model for desert dust intrusions occurred at Granada during 2005–2010 and for the corresponding clean atmosphere conditions (cloud and aerosol free conditions) for the three desert dust origin classes. The African dust intrusions over the study location caused an average decrease in the global solar radiation at surface of 7.1 % (sector A), 7.7 % (sector B), and 6.6 % (sector C), which means less energy reaching the ground and, therefore, more cooling of the ground. This decrease in the global radiation was due to the balance between the strong increase of the diffuse component (∼ 250 %) and the substantial reduction of the direct component (∼ 26 %). These large changes in direct and diffuse components point out the importance of the desert dust intrusions over South-Eastern Spain, indicating that this type of particles significantly affect the propagation of solar radiation through the atmosphere. Table 1 also shows the computed mean values of the upward radiation at TOA for desert dust intrusions and for the corresponding clear atmosphere conditions (cloud-free conditions and no presence of aerosol). The desert dust particles produced an increase in the upward radiation of 8.2 % (sector A), 10.3 % (sector B) and 9.4 % (sector C). These results revealed that desert dust particles produce a significant planetary cooling.

ACPD
12, 6593–6622, 2012

In order to avoid the AOD dependence of ARF, the aerosol radiative forcing efficiency (ARFE) which is the aerosol radiative forcing per unit of AOD (440 nm) was also investigated in this study. A simple method for calculating the aerosol radiative forcing efficiency, ARFE, is to perform a linear regression between ARF and AOD (Yoon et al., 2005; Antón et al., 2011). The slope of best-fit line of ARF versus AOD is the ARFE. Figure 4 shows the relationship between surface and TOA instantaneous ARF and AOD (440 nm) for the three African desert dust origin classes considering SZA lower than 65 degrees. Table 2 shows the ARFE values at surface and TOA ($ARFE_{Surface}$ and $ARFE_{TOA}$) obtained in each dust origin class. The ARFE values at surface ranged from -157 ± 21 (Sector A) to $-147 \pm 23\,W\,m^{-2}$ (Sector C). These large $ARFE_{Surface}$ values indicated that the surface was deprived of a substantial amount of solar energy in the presence of Africa desert dust over the South-Eastern Spain. Additionally, the ARFE values at TOA changed from -40 ± 30 (Sector A) to $-50 \pm 30\,W\,m^{-2}$ (Sector C). The ARFE values obtained in sector A (slightly lower absolute value at the TOA and higher absolute value at the surface) were consistent with the results given by Valenzuela et al. (2012a) who showed that the value of single scattering albedo was lowest in this sector.

It is interesting to compare the results obtained here with results obtained during desert dust events in other regions. In Table 3 we present the ARF and ARFE values given by several authors for situations dominated by desert dust and for cases where dust is mixed with other aerosol types. The ARF values ranged from $2\,W\,m^{-2}$ (Kanpur, India) to $-21\,W\,m^{-2}$ (El Arenosillo, Spain) at TOA, from $-11\,W\,m^{-2}$ (Lampedusa, Italy) to $-130\,W\,m^{-2}$ (Central Africa) at surface, and from $\sim 4\,W\,m^{-2}$ (Lampedusa) to $\sim 55\,W\,m^{-2}$ (Toulon, France) in the atmosphere. The large differences in ARF between these sites may likely be related to the differences in the methods used, measurement periods, desert dust load, chemical composition of dust, aerosol mixing state and surface albedo.

The ARFE values found in our study were higher (in absolute value) than those obtained during desert dust intrusions in the sites presented in Table 3. The high ARFE

ACPD
12, 6593–6622, 2012

values at surface obtained during desert dust events occurred at Granada could be due to the significant contribution of anthropogenic pollutants (especially absorbing particles). In fact, during these desert dust events, Valenzuela et al. (2012a) reported values of ω_o (λ) (0.89 at 440 nm) lower than those reported in the literature for desert dust aerosols (e.g., Dubovik et al., 2002). Perrone and Bergamo (2011) also showed that the contribution of anthropogenic particles can be relevant during desert dust events over Mediterranean sites. These authors reported ω_o values at 550 nm in the range 0.87–0.95 at Lecce (40.33° N, 18.10° E) in the Central Mediterranean during desert dust events.

AERONET products are extensively used in aerosol-related research. Table 4 shows the overall averages of TOA and surface ARF provided by AERONET for desert dust events analyzed in this study (http://aeronet.gsfc.nasa.gov). For computing the ARF, AERONET uses the aerosol optical properties retrieved using almucantar sky radiance measurements. However, to determine the ARF presented in this study (Table 2) we have utilized SBDART model using as input the aerosol optical properties retrieved using sky radiance in principal plane configuration. Although the inversion procedures are different, it can be seen that in general the results were very similar (see Tables 2 and 4). In the three sector origins, the TOA aerosol radiative forcing calculated using SBDART model was slightly higher (in absolute value) than the given by AERONET. However, the AERONET aerosol radiative forcing at the surface in sector A was slightly higher (in absolute value) than the computed by SBDART model. The surface ARF values determined by AERONET and SBDART model were comparable in the other sectors. Therefore, the comparison showed a good agreement between the ARF derived from AERONET and SBDART model, pointing out the reliability of the results shown in this work.

ACPD
12, 6593–6622, 2012

5 Conclusions

Simulations of shortwave global irradiances during desert dust events at the South-Eastern Spain from 2005 to 2010 period have been used to derive the instantaneous aerosol radiative forcing and aerosol forcing efficiency. For that, experimental measurements of aerosol radiative properties have been utilized as input in these simulations. The consideration in the inversion code of non-spherical particles has allowed us to have more accurate measurements of optical and microphysical properties of atmospheric aerosol to reduce the uncertainty in their climatic effects.

The adequacy of the model output data by the SBDART radiative transfer code has been evaluated by comparison with surface global irradiance values obtained from CM-11 pyranometer measurement. The agreement was excellent, but the modeled values slightly overestimate the surface global solar irradiance data which could be mainly associated with errors in the model input parameters.

The seasonal changes of surface ARF in July and March were not consistent with AOD (440 nm). Probably, this is due to the lower aerosol spectral single scattering albedo values during those months. The small forcing at TOA from April to August and the large forcing at surface implies that less solar energy reached the ground and more energy went to the atmosphere during those months.

The ARF at TOA showed a strong dependence on SZA while the ARF at surface only presented a very slight SZA dependence. This behavior was equal for the three datasets according their desert dust origin sources. Nevertheless, the ARF values for the sector B were higher (in absolute term) than the ARF values for the other two sectors. This fact was related to higher columnar aerosol load for the sector B.

The evaluation of the aerosol forcing efficiency at the surface and at the TOA during desert dust events provides high values (absolute value) of this parameter when air masses were transported from all origin sectors. However, surface ARFE was slightly higher when air masses were transported from sector A. This result was consistent with lower single scattering albedo for this sector. In general, the analysis of the ARFE

ACPD
12, 6593–6622, 2012

during desert dust events provides higher values of this parameter respect to the most of the ARFE during desert dust intrusions listed in the bibliography. This results suggests that the aerosol over South-Eastern Spain during desert dust events was more absorbing than in others locations.

Finally, the agreement between SBDART computed and AERONET retrievals confirms the reliability of the code used in this work.

Acknowledgements. This work was supported by the Andalusia Regional Government through projects P08-RNM-3568 and P10-RNM-6299, by the Spanish Ministry of Science and Technology through projects CGL2010-18782, CSD2007-00067 and CGL2011-13580-E/CLI; and by EU through ACTRIS project (EU INFRA-2010-1.1.16-262254). The authors thankfully acknowledge the computer resources, technical expertise and assistance provided by the Barcelona Supercomputing Center. ALFA database computation was partly supported by RES (Spanish Supercomputation Network) computing resources (projects AECT-2009-1-0012, AECT-2011-3-0016).

References

Alados-Arboledas, L., Lyamani, H., and Olmo, F. J.: Aerosol size properties at Armilla, Granada (Spain), Q. J. Roy. Meteor. Soc., 129, 1395–1413, 2003.

Alados-Arboledas, L., Alcántara, A., Olmo, F. J., Martínez-Lozano, J. A., Estellés, V., Cachorro, V., Silva, A. M., Horvath, H., Gangl, M., Díaz, A., Pujadas, M., Lorente, J., Labajo, A., Sorribas, M., and Pavese, G.: Aerosol columnar properties retrieved from CIMEL radiometers during VELETA 2002, Atmos. Environ., 42, 2654–2667, 2008.

Antón, M., Gil, J. E., Fernández-Gálvez, J., Lyamani, H., Valenzuela, A., Foyo-Moreno, I., Olmo, F. J., and Alados-Arboledas, L.: Evaluation of the aerosol forcing efficiency in the UV erythemal range at Granada, Spain, J. Geophys. Res., 116, D20214, doi:10.1029/2011JD016112, 2011.

Bauer, S., Bierwirth, E., Esselborn, M., Petzold, A., Macke, A., Trautmann, T., and Wendisch, M.: Airborne spectral radiation measurements to derive solar radiative forcing of Saharan dust mixed with biomass burning smoke particles, Tellus B, 63, 742–750, 2011.

ACPD

12, 6593–6622, 2012

Bellantone, V., Carofalo, I., De Tomasi, F., Perrone, M. R., Santese, M., Tafuro, A. M., and Turnone, A.: In situ samplings and remote sensing measurements to characterize aerosol properties over South-East Italy, J. Atmos. Ocean. Tech., 25(8), 1341–1356, 2008.

Di Biagio, C., di Sarra, A., Meloni, D., Monteleone, F., Piacentino, S., and Sferlazzo, D.: Measurements of Mediterranean aerosol radiative forcing and influence of the single scattering albedo, J. Geophys. Res., 114, D06211, doi:10.1029/2008JD011037, 2009.

Carofalo, I., Fermo, P., Perrone, M. R., and Piazzalunga, A.: Advection patterns and composition of TSP and $PM_{2.5}$ samples over South-East Italy, Proc. Chem. Eng. Trans., 18, 185–192, 2008.

Cachorro, V. E., Toledano, C., Prats, N., Sorribas, M., Mogo, S., Berjón, A., Torres, B., Rodrigo, R., de la Rosa, J., and De Frutos, A. M.: The strongest desert dust intrusion mixed with smoke over the Iberian Peninsula registered with Sun photometry, J. Geophys. Res., 113, D14S04, doi:10.1029/2007JD009582, 2008.

Dubovik, O. and King, M. D.: A flexible inversion algorithm for retrieval of aerosol optical properties from sun and sky radiance measurements, J. Geophys. Res., 105, 20673–20696, 2000.

Dubovik, O., Holben, B. N., Lapyonok, T., Sinyuk, A., Mishchenko, M. I., Yang, P., and Slutsker, I.: Non-spherical aerosol retrieval method employing light scattering by spheroids, Geophys. Res. Lett., 29(N10), 1415, doi:10.1029/2001GL014506, 2002a.

Dubovik, O., Holben, B., Eck, T. F., Smirnov, A., Kaufman, Y. J., King, M. D., Tanre, D., and Slutsker, I.: Variability of absorption and optical properties of key aerosol types observed in worldwide locations, J. Atmos. Sci., 59, 590–608, 2002b.

Dubovik, O., Sinyuk, A., Lapyonok, T., Holben, B. N., Mishchenko, M., Yang, P., Eck, T. F., Volten, H., Muñoz, O., Veihelmann, B., van der Zande, W. J., Leon, J. F., Sorokin, M., and Slutsker, I.: Application of spheroid models to account for aerosol particle nonsphericity in remote sensing of desert dust, J. Geophys. Res., 111, D11208, doi:10.1029/2005JD006619, 2006.

Eck, T. F., Holben, B. N., Sinyuk, A., Pinker, R. T., Goloub, P., Chen, H., Chatenet, B., Li, Z., Singh, R. P., Tripathi, S. N., Reid, J. S., Giles, D. M., Dubovik, O., O'Neill, N. T., Smirnov, A., Wang, P., and Xia, X.: Climatological aspects of the optical properties of fine/coarse mode aerosol mixtures, J. Geophys. Res., 115, D19205, doi:10.1029/2010JD014002, 2010.

Foster, P., Ramaswamy, V., Artaxo, P., Berntsen, T., Betts, R., Fahey, D. W., Haywood, J., Lean, J., Lowe, D. C., Myhre, G., Nganga, J., Prinn, R., Raga, G., Schulz, M., and Van Dorland, R.: Changes in atmospheric constituents and in radiative forcing, in: Climate Change

ACPD
12, 6593–6622, 2012

2007: The Physical Science Basis, Contribution of Working Group I to the Fourth Assessment Report of the Intergovernmental Panel on Climate Change, edited by: Solomon, S., Qin, D., Manning, M., Chen, Z., Marquis, M., Averyt, K. B., Tignor, M., and Miller, H. L., Cambridge University Press, Cambridge, UK and New York, NY, USA, 2007.

Gangoiti, G., Alonso, L., Navazo, M., García, J. A., and Millán, M. M.: North African soil dust and European pollution transport to America during the warm season: hidden links shown by a passive tracer simulation, J. Geophys. Res., 111, D10109, doi:10.1029/2005JD005941, 2006.

Garcia, O. E., Exposito, F. J., Diaz, J. P., and Diaz, A. M.: Radiative forcing under mixed aerosol conditions, J. Geophys. Res., 116, D01201, doi:10.1029/2009JD013625, 2011.

Gerasopoulos, E., Andreae, M. O., Zerefos, C. S., Andreae, T. W., Balis, D., Formenti, P., Merlet, P., Amiridis, V., and Papastefanou, C.: Climatological aspects of aerosol optical properties in Northern Greece, Atmos. Chem. Phys., 3, 2025–2041, doi:10.5194/acp-3-2025-2003, 2003.

Holben, B. N., Eck, T. F., Slutsker, I., Tanre, D., Buis, J. P., Setzer, A., Vermote, E., Reagan, J. A., Kaufman, Y. J., Nakajima, T., Lavenu, F., Jankowiak, I., and Smirnov, A.: AERONET – a federated instrument network and data archive for aerosol characterization, Remote Sens. Environ., 66, 1–16, 1998.

Kandler, K., Benker, N., Bundke, U., Cuevas, E., Ebert, M., Knippertz, P., Rodríguez, S., Schütz, L., and Weinbruch, S.: Chemical composition and complex refractive index of Saharan Mineral Dust at Izaña, Tenerife (Spain) derived by electron microscopy, Atmos. Environ., 41, 8058–8074, 2007.

Kim, D. H., Sohn, B. J., Nakajima, T., and Takamura, T.: Aerosol radiative forcing over East Asia determined from ground-based solar radiation measurements, J. Geophys. Res., 110, D10S22, doi:10.1029/2004JD004678, 2005.

Koren, I., Ganor, E., and Joseph, J. H.: On the relation between size and shape of desert dust aerosol, J. Geophys. Res., 106, 18047–18054, 2001.

Kubilay, N., Cokacar, T., and Oguz, T.: Optical properties of mineral dust outbreaks over the Northeastern Mediterranean, J. Geophys. Res., 108(D21), 4666, doi:10.1029/2003JD003798, 2003.

Li, Z., Goloub, P., Devaux, C., Gu, X., Qiao, Y., Zhao, F., and Chen, H.: Aerosol polarized phase function and single scattering albedo retrieved from ground-based measurements, Atmos. Res., 71, 233–241, 2004.

ACPD
12, 6593–6622, 2012

Lyamani, H., Olmo, F. J., and Alados-Arboledas, L.: Saharan dust outbreak over Southeastern Spain as detected by sun photometer, Atmos. Environ., 39, 7276–7284, 2005.
Lyamani, H., Olmo, F. J., Alcántara, A., and Alados-Arboledas, L.: Atmospheric aerosols during the 2003 heat wave in Southeastern Spain I: spectral optical depth, Atmos. Environ., 40(33), 6453–6464, 2006a.
Lyamani, H., Olmo, F. J., Alcántara, A., and Alados-Arboledas, L.: Atmospheric aerosols during the 2003 heat wave in Southeastern Spain II: microphysical columnar properties and radiative forcing, Atmos. Environ., 40, 6465–6476, 2006b.
Lyamani, H., Olmo, F. J., and Alados-Arboledas, L.: Physical and optical properties of aerosols over an urban location in Spain: seasonal and diurnal variability, Atmos. Chem. Phys., 10, 239–254, doi:10.5194/acp-10-239-2010, 2010.
Meloni, D., di Sarra, A., Di Iorio, T., and Fiocco G.: Influence of the vertical profile of Saharan dust on the visible direct radiative forcing, J. Quant. Spectrosc. Ra., 93, 397–413, 2005.
Mishchenko, M. I., Travis, L. D., Kahn, R. A., and West, R. A.: Modeling phase functions for dustlike tropospheric aerosols using a shape mixture of randomly oriented polydisperse spheroids, J. Geophys. Res., 102, 16831–16847, 1997.
Muñoz, O., Volten, H., de Haan, J. F., Vassen, W., and Hovenier, J. W.: Experimental determination of scattering matrices of randomly oriented fly ash and clay particles at 442 and 633 nm, J. Geophys. Res., 106, 22833–22844, 2001.
Nakajima, T., Tonna, G., Rao, R. Z., Boi, P., Kaufman, Y., and Holben, B.: Use of sky brightness measurements from ground for remote sensing of particulate polydispersions, Appl. Optics, 35, 2672–2686, 1996.
Olmo, F. J., Quirantes, A., Alcantara, A., Lyamani, H., and Alados-Arboledas, L.: Preliminary results of a non-spherical aerosol method for the retrieval of the atmospheric aerosol optical properties, J. Quant. Spectrosc. Ra., 100, 305–314, 2006.
Olmo, F. J., Quirantes, A., Lara, V., Lyamani, H., and Alados-Arboledas, L.: Aerosol optical properties assessed by an inversion method using the solar principal plane for non-spherical particles, J. Quant. Spectrosc. Ra., 109, 1504–1516, 2008.
Otto, S., Bierwirth, E., Weinzierl, B., Kandler, K., Esselborn, M., Tesche, M., Schladitz, A., Wendisch, M., and Trautmann, T.: Solar radiative effects of a Saharan dust plume observed during SAMUM assuming spheroidal model particles, Tellus B, 61, 270–296, 2009.
Papayannis, A., Amiridis, V., Mona, L., Tsaknakis, G., Balis, D., Bösenberg, J., Chaikovski, A., De Tomasi, F., Grigorov, I., Mattis, I., Mitev, V., Müller, D., Nickovic, S., Pérez, C.,

ACPD
12, 6593–6622, 2012

Pietruczuk, A., Pisani, G., Ravetta, F., Rizi, V., Sicard, M., Trickl, T., Wiegner, M., Gerding, M., Mamouri, R. E., D'Amico, G., and Pappalardo, G.: Systematic lidar observations of Saharan dust over Europe in the frame of EARLINET (2000–2002), J. Geophys. Res., 113, D10204, doi:10.1029/2007JD009028, 2008.

Perrone, M. R. and Bergamo, A.: Direct radiative forcing during Sahara dust intrusions at a site in the Central Mediterranean: Anthropogenic particle contribution, Atmos. Res., 101, 783–798, doi:10.1016/j.atmosres.2011.05.011, 2011.

Pilinis, C. and Li, X.: Particle shape and internal inhomogeneity effects in the optical properties of tropospheric aerosols of relevance to climate forcing, J. Geophys. Res., 103(D4), 3789–3800, 1998.

Pinker, R. T., Liu, H., Osborne, S. R., and Akoshile, C.: Radiative effects of aerosols in sub-Sahel Africa: dust and biomass burning, J. Geophys. Res., 115, D15205, doi:10.1029/2009JD013335, 2010.

Prospero, J. M., Ginoux, P., Torres, O., Nicholson, S. E., and Gill, T. E.: Environmental characterization of global sources of atmospheric soil dust identified with the Nimbus 7 Total Ozone Mapping Spectrometer (TOMS) absorbing aerosol product, Rev. Geophys., 40, 1002, doi:10.1029/2000RG000095, 2002.

Ricchiazzi, P., Yang, S., Gautier, C., and Sowle, D.: SBDART: a research and teaching software tool for plane-parallel radiative transfer in the Earth's atmosphere, B. Am. Meteorol. Soc., 79, 2101– 2114, 1998.

Rodríguez, S., Alastuey, A., Alonso-Pérez, S., Querol, X., Cuevas, E., Abreu-Afonso, J., Viana, M., Pérez, N., Pandolfi, M., and de la Rosa, J.: Transport of desert dust mixed with North African industrial pollutants in the subtropical Saharan Air Layer, Atmos. Chem. Phys., 11, 6663–6685, doi:10.5194/acp-11-6663-2011, 2011.

Sokolik, I. N. and Toon, O. B.: Incorporation of mineralogical composition into models of the radiative properties of mineral aerosol from UV to IR wavelengths, J. Geophys. Res., 104, 9423–9444, 1999.

Stamnes, K., Tsay, C., Wiscombe, W., and Jayaweera, K.: Numerically stable algorithm for discrete-ordinate-method radiative transfer in multiple scattering and emitting layered media, Appl. Optics, 27, 2502–2509, 1988.

Tafuro, A. M., Barnaba, F., De Tomasi, F., Perrone, M. R., and Gobbi, G. P.: Saharan dust particle properties over the central Mediterranean, Atmos. Res., 81, 67–93, 2006.

Tesche, M., Ansmann, A., Müller, D., Althausen, D., Mattis, I., Heese, B., Freudenthaler, V.,

ACPD
12, 6593–6622, 2012

Wiegner, M., Esselborn, M., Pisani, G., and Knippertz, P.: Vertical profiling of Saharan dust with Raman lidars and airborne HSRL in Southern Morocco during SAMUM, Tellus B, 61, 144–164, 2009.

Toledano, C., Cachorro, V. E., de Frutos, A. M., Sorribas, M., Prats, N., and de la Morena, B. A.: Inventory of African desert dust events over the Southwestern Iberian Peninsula in 2000–2005 with an AERONET Cimel Sun photometer, J. Geophys. Res., 112, D21201, doi:10.1029/2006JD008307, 2007.

Valenzuela, A., Olmo, F. J., Lyamani, H., Antón, M., Quirantes, A., and Alados-Arboledas, L.: Analysis of the desert dust radiative properties over Granada using principal plane sky radiances and spheroids retrieval procedure, Atmos. Res., 104–105, 292–301, 2012a.

Valenzuela, A., Olmo, F. J., Lyamani, H., Antón, M., Quirantes, A., and Alados-Arboledas, L.: Classification of aerosol radiative properties during African desert dust intrusions over Southeastern Spain by sector origins and cluster analysis, J. Geophys. Res., doi:10.1029/2011JD016885, in press, 2012b.

Vermeulen, A., Devaux, C., and Herman M.: Retrieval of the scattering and microphysical properties of aerosols from ground.based optical measurements including polarization. I. Method, Appl. Optics, 39, 6207–6220, 2000.

Wagner, F., Bortoli, D., Pereira, S., Costa, M. J., Silva, A. M., Weinzierl, B., Esselborn, M., Petzold, A., Rasp, K., Heinold, B., and Tegen, I.: Properties of dust aerosol particles transported to Portugal from the Sahara desert, Tellus B, 61, 297–306, 2009.

Won, J.-G., Yoon, S.-C., Kim, S.-W., Jefferson, A., Dutton, E. G., and Holben, B. N.: Estimations of direct radiative forcing of Asian dust aerosols with sun/sky radiometer ans lidar measurements at Gosan, Korea, J. Meteorol. Soc. Jpn., 82, 115–130, 2004.

Yang, P., Feng, Q., Hong, G., Kattawar, G. W., Wiscombe, W. J., Mishchenko, M. I., Dubovik, O., Laszlo, I., and Sokolik, I. N.: Modeling of the scattering and radiative properties of nonspherical dust particles, J. Aerosol Sci., 38, 995–1014, 2007.

Yoon, S. C., Won, J. G., Omar, A. H., Kim, S. W., and Sohn, B. J.: Estimation of the radiative forcing by key aerosol types in worldwide locations using a column model and AERONET data, Atmos. Environ., 39, 6620–6630, 2005.

ACPD
12, 6593–6622, 2012

Table 1. SBDART computed irradiances for desert dust intrusions occurred at Granada during 2005–2010 and for the corresponding no-aerosol conditions for the three desert dust origin classes.

Source region	Conditions	Irradiances ($W\,m^{-2}$)			
		Surface			TOA
		Direct	Diffuse	Global	Upward radiation
Sector A	desert	478 ± 224	175 ± 79	653 ± 251	146 ± 31
	no-aerosol	653 ± 247	50 ± 7	703 ± 254	135 ± 36
Sector B	desert	447 ± 211	194 ± 73	642 ± 251	148 ± 31
	no-aerosol	645 ± 247	50 ± 7	695 ± 254	134 ± 36
Sector C	Desert	474 ± 210	176 ± 63	650 ± 234	147 ± 28
	no-aerosol	645 ± 228	51 ± 6	696 ± 234	135 ± 35

ACPD
12, 6593–6622, 2012

Table 2. Aerosol radiative forcing ($W\,m^{-2}$) and aerosol radiative forcing efficiency ($W\,m^{-2}$ per unit of AOD (440 nm)) at surface, TOA and in the atmosphere during desert dust events occurred at Granada during 2005–2010 period for sector A, B and C.

Source region	ARF_{TOA}	$ARF_{Surface}$	$ARF_{Atmosphere}$	$ARFE_{TOA}$	$ARFE_{Surface}$
Sector A	-11 ± 13	-43 ± 26	33 ± 21	-39 ± 34	-157 ± 21
Sector B	-14 ± 12	-46 ± 17	32 ± 16	-46 ± 34	-154 ± 23
Sector C	-13 ± 11	-39 ± 19	27 ± 18	-49 ± 34	-147 ± 23

ACPD
12, 6593–6622, 2012

Table 3. Aerosol radiative forcing ($W\,m^{-2}$) and forcing efficiency ($W\,m^{-2}$ per unit of AOD) at surface, TOA and in the atmosphere observed over different locations.

Reference Location	Aerosol Type	ARF_{TOA}	$ARF_{Surface}$	$ARF_{Atmosphere}$	$ARFE_{TOA}$	$ARFE_{Surface}$	
Meloni et al. (2005)	Dust	−5.1 to −8.7	−11.0 to −14.2	3.7 to 9	−15.0 to −16.4	−28.4 to −30.1	Lampedusa, Italy
	Dust	−3.1 to −5.2	−11.9 to −18.9	8.8 to 15.8	−8.6 to −10.0	−42.9 to −45.6	Lampedusa, Italy
Cachorro et al. (2008)	Dust + smoke	−21 −39	–	−55.6	−120	El Arenosillo, Spain	
Derimian et al. (2008)	Dust + Biomass Burning	−5.2	−42.0	36.8	−5.6	−45.0	M'Bour, Senegal
	Dust	−8.1	−29.1	21.0	−15.7	−56.4	M'Bour, Senegal
Di Biagio et al. (2009)	Dust	–	–	–	–	−82 to −185	Lampedusa, Italy
Prasad et al. (2007)	Dust	2 to −26	−19 to −87	–	−17 ± 2.5	−46 ± 2.6	Kanpur, India
Perrone et al. (2011)	Dust	−11 to −25	−25 to −53	–	−52 to −82	−122 to −155	Lecce, Italy
Saha et al. (2008)	Dust	−7.7 to −9.8	−61.8 to −64.4	54.1 to 54.6	−9.7 to −12.4	−78.2 to −81.5	Toulon, France
Garcia et al. (2011)	Dust	−38 ± 18	−88 ± 41	–	–	–	Central Africa Region
	Dust + Biomass Burning	−34 ± 18	−130 ± 41	–	–	–	Central Africa Region

ACPD
12, 6593–6622, 2012

Table 4. AERONET aerosol radiative forcing ($W\,m^{-2}$) at surface and TOA during desert dust events occurred at Granada from 2005 to 2010 for sectors A, B and C.

Source origin	ARF_{TOA}	$ARF_{Surface}$
Sector A	-10 ± 12	-46 ± 21
Sector B	-11 ± 10	-45 ± 17
Sector C	-12 ± 7	-40 ± 14

ACPD
12, 6593–6622, 2012

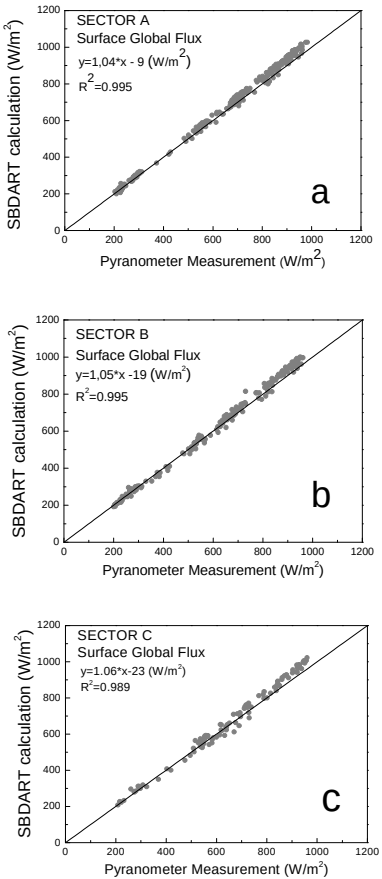

Fig. 1. Comparisons of surface global irradiance measurements obtained during desert dust events occurred at Granada during 2005–2010 with SBDART modeled results for **(a)** sector A, **(b)** sector B and **(c)** sector C.

ACPD
12, 6593–6622, 2012

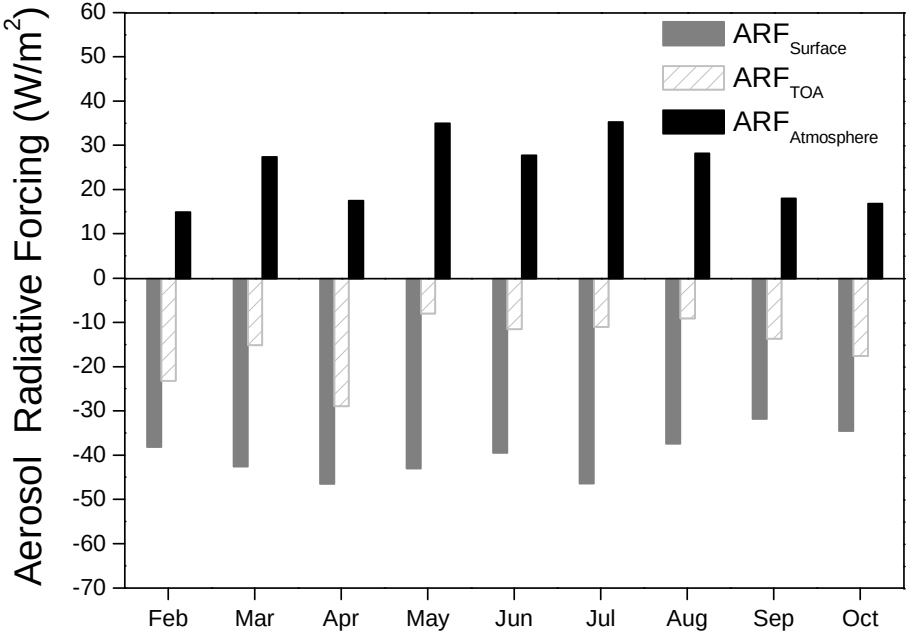

Fig. 2. Monthly mean evolutions of aerosol radiative forcing at TOA, surface and in the atmosphere during desert dust events occurred at Granada during 2005–2010.

ACPD
12, 6593–6622, 2012

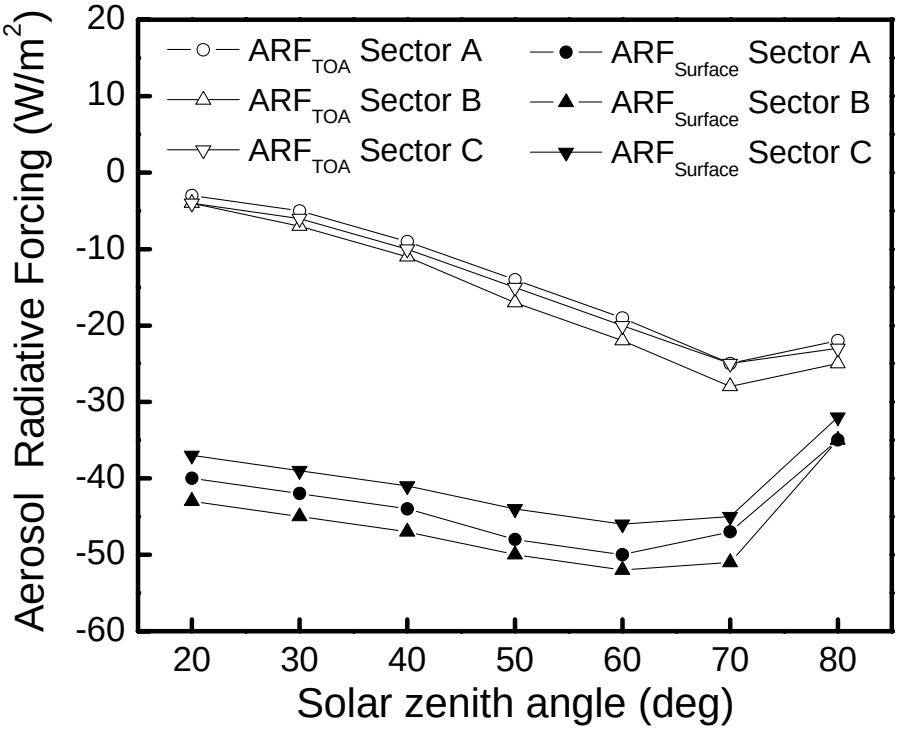

Fig. 3. Computed aerosol radiative forcing at TOA (open symbols) and at surface (full symbols) as a function of solar zenith angle for the sectors A, B and C during desert dust events occurred at Granada from 2005 to 2010.

ACPD
12, 6593–6622, 2012

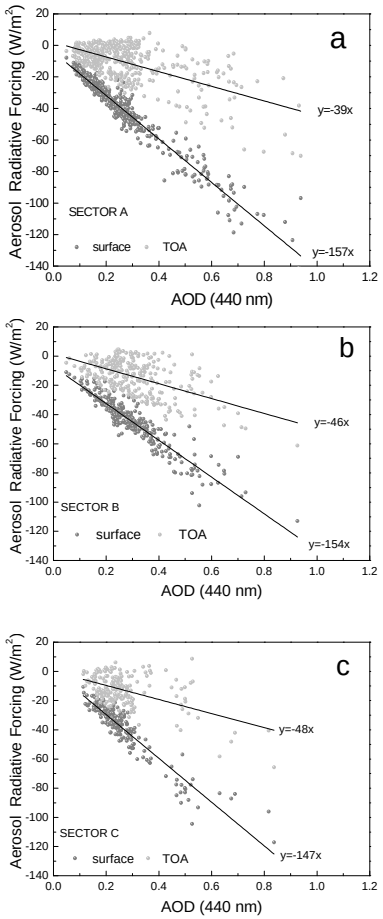

Fig. 4. The relation between surface and TOA Aerosol radiative forcing and AOD (440 nm) during desert dust events occurred at Granada during 2005–2010 for **(a)** sector A, **(b)** sector B and **(c)** sector C.

ACPD
12, 6593–6622, 2012